Food Chemistry 405 (2023) 134713

Contents lists available at ScienceDirect

Food Chemistry

journal homepage: www.elsevier.com/locate/foodchem

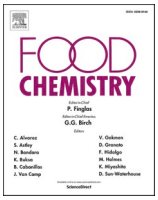

EC-SERS detection of thiabendazole in apple juice using activated screen-printed electrodes

Rebeca Moldovan [a], Karolina Milenko [b], Elizaveta Vereshchagina [b], Bogdan-Cezar Iacob [a], Kenneth Schneider [c], Cosmin Farcău [d], Ede Bodoki [a,*]

[a] Analytical Chemistry Department, Faculty of Pharmacy, "Iuliu Haţieganu" University of Medicine and Pharmacy, 4, Louis Pasteur, 400349 Cluj-Napoca, Romania
[b] Department of Smart Sensors and Microsystems, SINTEF Digital, Gaustadalléen 23C, 0373 Oslo, Norway
[c] Department of Process Technology, SINTEF Industry, Forskningsveien 1, 0373 Oslo, Norway
[d] National Institute for Research and Development of Isotopic and Molecular Technologies, 67-103 Donat, 400293 Cluj-Napoca, Romania

ARTICLE INFO

Keywords:
Thiabendazole
Electrochemical roughening
Spectroelectrochemistry
Microfluidics
Miniaturized flow cell
Apple juice

ABSTRACT

Thiabendazole (TBZ), a benzimidazole fungicide used for post-harvest treatment, may be a trace contaminant of food matrices. In this work, we report the first EC-SERS (electrochemical-surface enhanced Raman spectroscopy) detection of TBZ in spiked apple juice using electrochemically (EC) roughened, gold-based screen-printed electrodes (AuSPEs) and portable instrumentation. Polarizing the substrate (−0.8 V vs Ag/AgCl) improves the recorded SERS signal of TBZ, allowing to reach a limit of detection (LOD) in juice of 0.061 ppm with a relatively wide linear range (0.5–10 μM) and good intermediate precision (%RSD < 10). The recovery of TBZ from unprocessed juice was found to be more than 82 %. Furthermore, a proof-of-concept integration of AuSPEs with a miniaturized flow cell for the preconcentration of TBZ and the controlled delivery of sample and reagents has been demonstrated. This approach paves the way for integrated, portable analytical systems applicable for on-site sample collection, processing, and analysis.

1. Introduction

TBZ is a benzimidazole pesticide commonly used in the post-harvest treatment of various fruits, such as apples, bananas, pears and citrus (Abad, Manclús, Moreno, & Montoya, 2001). The fruits are usually drenched or dipped in TBZ wax emulsions before storage. This treatment step prevents contamination with a wide range of fungi (e.g. Aspergillus, Botrytis) that are harmful to human health ("Revision of the Review of the Existing Maximum Residue Levels for Thiabendazole," 2016). However, there are also numerous negative health effects that have been associated with exposure to pesticides. TBZ was listed in the top 10 most frequently found pesticides in human foods by the U.S. Food and Drug Administration (FDA) in 2019 (Pesticide Residue Monitoring Report and Data for FY 2019 | FDA, n.d.). The penetrability of TBZ through the fruits' skin is not well established and washing cannot remove it completely from the treated surface (Müller, David, Chiş, & Pînzaru, 2014). Hence, it is often found as a residue in various foods, including fruit juices. Although TBZ is recognized of having low acute toxicity, at high doses causing disturbance of the thyroid hormone balance, it is classified as likely to be carcinogenic by the US Environmental Protection Agency (EPA) (EPA Office of Pesticide Programs, n.d.). Therefore the European Food Safety Authority (EFSA) reports maximum residual limits (MRL) of 4 mg/kg for TBZ in apples (EU Pesticides Database, n.d.).

Separation techniques such as gas chromatography (GC) or high-performance liquid chromatography (HPLC) coupled with fluorescence, UV or mass spectrometric (MS) detection are usually employed to detect pesticides residues, including TBZ, from different matrices (Albero, Sánchez-Brunete, & Tadeo, 2004; Sannino, 2008). These conventional techniques are sensitive and accurate, but they require extensive sample pretreatment, expensive equipment, and usually, they imply lengthy analysis processes.

In this context, novel analytical methods for TBZ analysis from fruit

Abbreviations: AuSPEs, gold screen-printed electrodes; CE, counter/auxiliary electrode; CV, cyclic voltammetry; EC, electrochemistry; EC-SERS, electrochemical-surface enhanced Raman spectroscopy; EPA, US Environmental Protection Agency; FDA, Food and Drug Administration; LOD, limit of detection; MRL, maximum residual limits; PBS, phosphate buffer saline; RE, reference electrode; RSD, relative standard deviation; SERS, surface enhanced Raman spectroscopy; SPEs, screen-printed electrodes; TBZ, thiabendazole; WE, working electrode.

* Corresponding author.
E-mail address: bodokie@umfcluj.ro (E. Bodoki).

https://doi.org/10.1016/j.foodchem.2022.134713
Received 26 May 2022; Received in revised form 8 September 2022; Accepted 19 October 2022
Available online 26 October 2022

derived products that are as sensitive, but cost-effective, time-effective, and user-friendly are of high demand. SERS is one of the most promising detection techniques in this regard, enabling enhancement of the Raman fingerprint signal amplitude by several orders of magnitude (Ru & Etchegoin, 2008). However, development of SERS applications is hampered by the lack of SERS substrates that are simultaneously accessible, reproducible, and provide high SERS enhancement factors. Generally, SERS substrates with very high enhancement factors may suffer from poor reproducibility (Liu et al., 2020), while very consistent and reproducible substrates tend to exhibit low enhancement factors. Screen-printed electrodes (SPEs), designed and mass-produced for various electroanalytical purposes, represent a promising compromise. They have all three electrodes needed for EC-SERS analysis integrated on the same chip: working electrode (WE), reference electrode (RE) and counter/auxiliary electrode (CE). Moreover, they are low-cost and they exhibit rather good batch-to-batch uniformity. Additionally, the WE may show very good SERS properties, particularly after a surface modification or an activation procedure. An example of surface modification is the decoration with noble metal nanostructures using a straightforward drop-coating method (Robinson, Harroun, Bergman, & Brosseau, 2012; Zhao, Blackburn, & Brosseau, 2015). Another convenient approach is the EC activation, i.e. physical surface roughening of noble metal SPEs (Ibáñez, González-García, Hernández-Santos, & Fanjul-Bolado, 2021; Wu, Li, Ren, & Tian, 2008). The EC activation procedure usually involves applying an oxidation–reduction cycle in an electrolyte solution that leads to atomic restructuring of the surface. An additional benefit of SPEs is the possibility to enhance the analytical performance by influencing the electromagnetic and chemical enhancement through modulation of the EC potential during the SERS measurements. In such EC-assisted SERS applications the interaction between the substrate and the target molecule, mandatory for a strong SERS effect, can improve multiple measurement aspects, such as selectivity (Bindesri, Alhatab, & Brosseau, 2018), adsorption of the analyte (Lynk, Sit, & Brosseau, 2018), and reproducibility (Huang & Hsiao, 2020). In the last few years, coupling SERS to electrochemistry emerged as an advantageous approach for detection and quantification of a large variety of analytes at trace levels, such as xenobiotics (Bindesri, Jebailey, Albarghouthi, Pye, & Brosseau, 2020; Velička, Zacharovas, Adomavičiūtė, & Šablinskas, 2021), biomarkers (Huang & Hsiao, 2020; Lynk et al., 2018), environmental pollutants (Ibáñez et al., 2021) or food contaminants (Robinson et al., 2012). EC-SERS proved to be suitable for analyses in several complex samples like saliva (Velička et al., 2021), urine (Hernandez, Perales-Rondon, Heras, & Colina, 2019), serum (Mohammadniaei, Yoon, Lee, & Choi, 2018), plasma (Hassanain, Izake, & Ayoko, 2018) and even milk (Sarfo et al., 2019).

To the best of our knowledge, EC-assisted SERS detection of TBZ has not been reported and only a limited number of publications address SERS detection of TBZ in juice samples, employing procedures that rely on laborious sample pretreatment steps and statistical analysis (Alsammarraie et al., 2018; Feng, Hu, Grant, & Lu, 2018) or time-consuming standard addition procedures (Chen et al., 2022). In this work, we report the first direct EC-assisted SERS detection of TBZ in supplemented apple juice, using AuSPEs activated by a new EC method. The potential-dependent and pH-dependent SERS response of TBZ were also investigated. Furthermore, we report the successful preconcentration and detection of TBZ at the surface of the EC-SERS sensor with the help of miniaturized flow cells.

2. Materials and methods

2.1. Materials

2.1.1. Chemicals and reagents

Thiabendazole (≥99 %), phosphate buffer solution 0.1 M, potassium chloride (≥99 %), $K_3Fe(CN)_6$ (≥99 %) and $K_4Fe(CN)_6$ (≥98.5 %) were provided by Sigma-Aldrich (St. Louis, USA). Boric acid (99.99 %), phosphoric acid (85 wt% in H_2O, 99.99 %) and sodium hydroxide (≥98 %) were provided by Merck (Darmstadt, Germany). Acetic acid (≥99.8 %) was provided by Fluka (North Carolina, USA). AuSPEs (BVT-AC1.W1.R1) were purchased from Palmsens (Houten, Netherlands). AuSPEs consist of three electrodes: Au WE (d.i. = 1 mm), Ag/AgCl (60 %/40 %) RE and Au CE. Apple juice (pH 5) was purchased from the local stores. The spiked juice samples used to demonstrate TBZ detection were prepared by adding known amounts of TBZ to juice. Specifically, aliquots of 5×10^{-5} M standard TBZ in PBS were added to the corresponding volumes of apple juice in order to reach 7.5×10^{-7} M and 7.5×10^{-6} M TBZ in the juice matrix.

Phosphate buffer saline (PBS) solution consisted of 0.05 M phosphate buffer and 0.1 M potassium chloride. Britton-Robinson (BR) buffer was prepared by adding 0.2 M sodium hydroxide to a mixture of 0.04 M boric acid, 0.04 M phosphoric acid and 0.04 M acetic acid until the desired pH was reached.

Stock solutions of 1 mM TBZ were prepared in ethanol. Working solutions were prepared from the stock solution upon dilution with either 0.05 M PBS, or with BR buffer to reach different concentrations of TBZ (down to 10^{-7} M) and stored at + 8 °C. Ultra-pure water (18.2 MΩ·cm) was used throughout the experiments.

2.1.2. Instrumentation

For SERS measurements a portable BWS465-785S i-Raman Plus spectrometer, resolution < 4.5 cm^{-1} @ 912 nm (BWTek, Delaware, USA), equipped with a high quantum efficiency CCD array detector, a fiber optic probe with 785 nm excitation wavelength and the BWSpec software for data collection and analysis was used. Different laser powers and acquisition times were used, as specified at the corresponding experiments.

For electrochemical activation of AuSPEs and EC-assisted SERS measurements a portable PalmSens4 (Palmsens, Houten, Netherlands) potentiostat and the PSTrace software for data collection and analysis was employed. All potentials were measured against the integrated Ag/AgCl reference electrode.

Scanning electron microscopy (SEM) images were obtained by using an ultra-high-resolution Hitachi 8230 system operated in high vacuum conditions.

2.2. Electrochemical characterization and activation of AuSPEs

The electrochemical properties of the AuSPEs were investigated before and after EC activation using cyclic voltammetry (CV) in 10 mM $[Fe(CN)_6]^{3-/4-}$ as redox probe and 100 mM KCl as supporting electrolyte.

In order to EC roughen the surface of AuSPEs, two potential steps were applied on the WE, with +1 V held for 30 s, closely followed by −0.52 V for another 30 s in quiescent 0.1 M KCl solution. Upon this electrode polarization process, the surface gold atoms are oxidized and rapidly reduced to restructure the surface at the nanoscale level. Reproducibility of the activation procedure was confirmed by recording both the SERS spectra (without applied potential) and the EC-assisted SERS spectra (at −0.8 V) of three different EC roughened AuSPEs in 0.1 mM TBZ solution in PBS. The height of the characteristic Raman band of TBZ at 786 cm^{-1} was considered.

2.3. EC-SERS analyses

For SERS and EC-assisted SERS analysis of TBZ in PBS and juice samples, a 30 s integration time (for potential-dependent SERS measurements 10 s) and a 20 % (68 mW) laser power was used, recording the average of 2 spectra. A home built XYZ positioning stage was employed to align the AuSPEs substrate to the focal point of the fiber probe. The pH dependence of the recorded SERS signal was studied on AuSPEs exposed for 10 min in 0.1 mM TBZ solution under magnetic stirring to make sure that the gold surface is saturated with the pesticide molecules (Oliveira,

Rubira, Furini, Batagin-Neto, & Constantino, 2020). All measurements were done in triplicate, except the pH dependency measurements, which were done in duplicate.

Samples of 70 μL were confined with a Viton O-ring between the active area of AuSPEs and a cover glass slip (thickness ca. 160 μm) to ensure measurement consistency by preventing evaporation and laser beam dispersion due to droplet convexity.

2.4. Microfluidic flow cell

The channels (1 mm wide) and fluidic chamber were cut in a pressure sensitive adhesive (PSA, art. 7840, Arcare®, thickness ca. 86 μm) using a Cameo Silhouette 3 cutter. The PSA was applied on the AuSPE sensor substrate. The top substrate, 1 mm thick poly(methyl methacrylate) (PMMA) plate, with inlets and outlets was attached on top, applying manual pressure.

The sensor was assembled to complete the microfluidic flow cell as shown in the Figure S1. AutoCAD 2021 was used for the 2D/3D designs of the fluidic chamber/channels. The channel width was 1 mm, limited by the resolution of the cutter. The diameter of the fluidic chamber is approx. 6 mm ensuring sufficient exposure of the circular electrodes. The height of the channel/chamber (equal to the thickness of the PSA after removing the liners) was ca. 86 μm, defining a volume above the active surface of the sensor of approx. 2.4 μL.

A programmable Harvard PHD 2000 syringe pump was used for flow control. The 20 mL BD Plastipak™ syringes with luer tips were equipped with a luer adapter and a silicon tubing. On the chip's side, the fluidic connectors (art. 10,000,700 from Microfluidic ChipShop) were installed in inlet/outlet ports and secured using an adhesive ring (art. 10000717). As specified by the manufacturer the Harvard Apparatus PHD 22/2000 syringe pump gives flow rate accuracy within 0.35 %; moreover, in our experiments flow was allowed to stabilize to ensure equal flow conditions between the experiments.

AuSPEs were first EC activated and then assembled with a top part and PSA to complete the microfluidic cell. The cell was filled with 10^{-5} M TBZ solution and SERS or EC-SERS experiments were performed both in static and flow cell configuration (Figure S2). To observe the dynamic accumulation of TBZ molecules at the gold surface during controlled flow, SERS spectra were recorded every 10 s at 20 % power (68 mW) for a total time of 30 min.

3. Results and discussion

3.1. Characterization of working electrode

3.1.1. Morphological characterization

The EC activation of AuSPEs was done in a double-step chronoamperometric procedure which implied oxidizing the surface gold atoms followed by their rapid electrodeposition (Figure S3) which enriched the rough electrode surface with sub-micron topographical features (Figure S4). Elemental analysis performed on electrodes before and after activation indicate an increase of the Au weight% induced by the EC activation (Figure S5). The Au amount increases with about 9 % (relative to its initial value), while the content of C and O atoms decreases. It is informative to analyze the Au/C ratio, which starts at 2.17 and increases to 2.71, while the Au/O ratio starts from 9.38 and increases to 14.5 on the activated electrodes. These results confirm that the supplementary nanoscale roughness observed in SEM images is indeed given by Au. These nanoscale features are expected to produce a twofold benefit: their size should favor SERS enhancements, while the associated increased surface area favors EC analyses. The double-step chronoamperometric procedure used above proved to be very efficient, probably because the gold ions formed during the anodic step were not able to diffuse away into the bulk solution before being reduced. Macroscopic optical images (photographs) of the AuSPEs electrodes show a change in color (inset from figure S4) after activation, an effect which implies the change of the microscopic surface features. The finer nanoscale particles on the activated electrode are more efficient in trapping light due to surface plasmon excitation, reducing the amount of reflected light and thus causing the darker appearance of the activated electrode.

3.1.2. Electrochemical characterization

The EC behavior of the electrode improves after activation. The recorded peak separation potential ($\Delta E_p = E_{pa}$ - E_{pc}) of the employed redox mediator decreases from 144 to 81 mV, whereas the anodic and cathodic peak currents increase with more than 30 % (Figure S6). The anodic and cathodic peak currents show linear correlation to the square root of the scan rate, indicating diffusion-controlled EC processes (Figure S7). The same linear correlation is observed from the log plot (anodic peak current vs scan rate) for all tested electrodes, with slope values close to 0.5, characteristic for diffusion-controlled processes.

The EC active surface area (A_{EA}) and roughness factor (R_f) of the AuSPEs before and after the activation procedure were also determined. Considering the quasi-reversibility of the heterogenous electron transfer process, confirmed by the linear trend of I_p versus $\nu^{1/2}$ plot shown in Figure S7, the Randles-Sevçik formula was used (supplementary information) in order to estimate the active surface areas of the electrodes (Salinas-Torres, Huerta, Montilla, & Morallón, 2011). Calculated values for A_{EA} and R_f show an approximately 48 % increase of these parameters upon the electrochemical activation of AuSPEs. The results prove that the EC roughening procedure has a positive impact on the electron transfer occurring at the electrode surface and the overall kinetics of the process, by creating a gold nanostructured surface and thus inducing a higher A_{EA}.

3.2. Potential and pH-dependent SERS spectra of TBZ

The Raman spectrum of the pure TBZ, presented in Figure S8, reveals various vibrational bands that contribute to the molecular fingerprint of this molecule (Müller et al., 2014). The most pronounced band at 1581 cm^{-1} are mainly attributed to stretching C—C vibrations in ring 2 and 3, stretching C═C vibrations in ring 3, stretching N═C vibrations in ring 2 and bending C—H and C—N—H in ring 2. The band at 1016 cm^{-1} is assigned to stretching C—N mode in ring 2 and C—C in ring 2 and 3 along with bending mode N═C-N group in ring 2 and 3. Another prominent resonance band at 1283 cm^{-1} is assigned to total ring stretching vibrations. The peak at 784 cm^{-1} was derived from S—C stretching vibrations and bending C═N and C—N vibrations in ring 1.

The potential-dependent SERS spectra for TBZ molecules were also recorded since, as to date, no previous data has been reported in the literature. Upon the polarization of the electrode in the range of 0 to − 1 V in 100 mV increments, the strongest signal enhancement on activated AuSPEs was observed at − 0.8 V (Fig. 1A). Various band intensity increases or decreases, or small band position shifts were observed in the TBZ SERS spectra at these negative potentials. In contrast, the SERS intensity for TBZ decreases dramatically at positive potentials, probably due to desorption of TBZ molecules by a positively charged surface, phenomenon which requires further investigation. Therefore, further spectroelectrochemical studies were conducted at the optimum potential of − 0.8 V (vs Ag/AgCl), for which the Raman bands at 786 cm^{-1} and 1012 cm^{-1} at open circuit potential (OCP) (shifted to 784 cm^{-1} and 1010 cm^{-1} at − 0.8 V) gain intensity and become the most prominent in the spectrum. Fig. 1B shows a comparison between the SERS spectra at OCP and the EC-SERS spectra at − 0.8 V (vs Ag/AgCl). A comparison of vibrational assignments for the characteristic Raman bands of TBZ for pure solid substance, SERS and EC-assisted SERS spectra are presented in detail in Table S1.

According to the SERS selection rules (Aroca, 2007), the scattering by vibrational modes perpendicular to the metallic surface would be amplified to a larger extent in SERS measurements. Several authors suggested that a perpendicular orientation of TBZ molecule on the

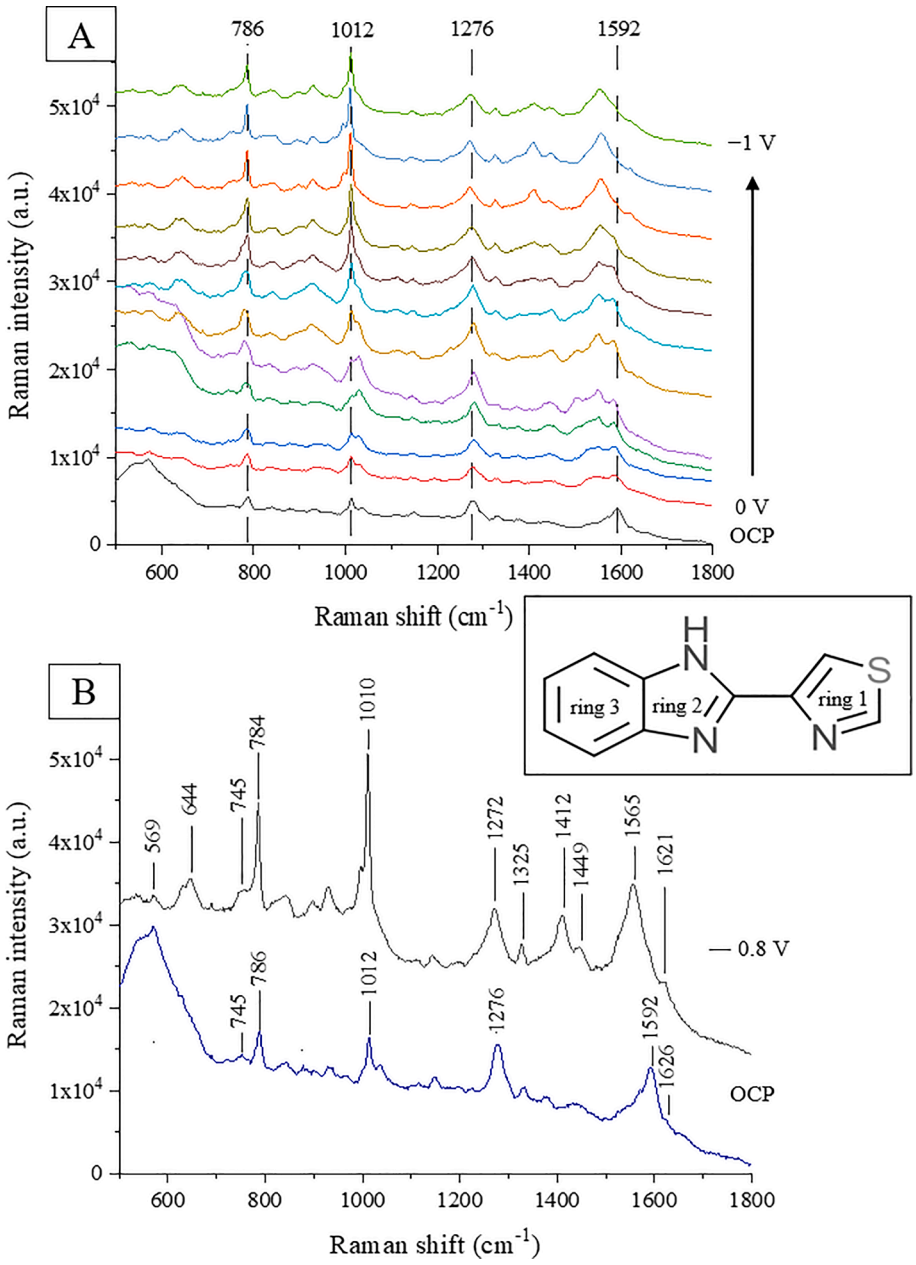

Fig. 1. Potential dependent SERS spectra of 10^{-5} M TBZ in PBS (pH 7) from OCP to −1 V in 100 mV increments (A) and SERS spectrum of TBZ at OCP (blue line) compared to EC-SERS spectrum at −0.8 V (black line) in PBS solution at pH 7 (B). Inset showing the chemical structure of thiabendazole. (For interpretation of the references to color in this figure legend, the reader is referred to the web version of this article.)

metallic surface could occur via an interaction between the sulfur atom (S) in ring 1 (Oliveira et al., 2020). At the same time, such a planar molecule should have the rather obvious tendency to lie flat on metallic surfaces, interacting with the metal via the delocalized π electrons in the planar rings (Kim, Kim, Lee, Jung, & Lee, 2009). On the other hand, the applied potential can determine modifications of SERS spectra even without involving any molecule reorientation on the metal surface: the bonding interaction of the molecule with the surface can be modified, which can slightly alter the geometric and electronic structure of the molecule, eventually leading to modifications of the molecule polarizability, thus also its Raman tensor, and finally the SERS spectrum. It is therefore difficult to confidently attribute the effects induced by the applied potential to one or more factors, without performing dedicated experiments, which is beyond the scope of the current study. However, we can only try to speculate that the increase in intensity of some bands and the decrease of others could imply a (partial) reorientation of the TBZ molecules on the surface. Since both the 784 cm^{-1} and 1010 cm^{-1} bands involve strong stretching vibrations along the short axis of TBZ (Fig. 1B, inset), a tilt of the molecule would seem conceivable.

The reproducibility of the EC roughening procedure was investigated by SERS with and without EC assistance (−0.8 V). A relative standard deviation (%RSD) of 21.3 % and 9 % was obtained on activated electrodes (n = 3) for the SERS and for the EC-assisted SERS measurements, respectively, suggesting that a potentiodynamic modulation of the electrode's surface leads to a more uniform SERS response.

As fruit juices intended for testing for their residual TBZ content imply variable acidity levels, the SERS and EC-SERS intensity dependence on pH changes was also monitored for TBZ (Figure S9). An ideal pH range of 4 to 7 was identified, where the polarization of the electrode/substrate (−0.8 V) resulted in optimum signal intensity enhancement. At more extreme pH values (2, 3 and 8), a decrease in EC-SERS intensity was observed compared to the SERS signal at OCP, with

the bands for TBZ disappearing almost completely at pH 2. Nevertheless, within the range of pH 4–7, the signal intensity and spectral features of TBZ are relatively constant. Other studies have also reported the pH dependent SERS behavior of TBZ, but limited to the Raman band shift and molecular orientation on Ag colloidal nanoparticles (Müller et al., 2014) or a very general report on the changes in intensity for three characteristic bands (782 cm^{-1}, 1008 cm^{-1}, 1578 cm^{-1}), without addressing the electric field effect (Chen et al., 2022).

3.3. SERS detection of TBZ in real samples

After the characterization of the electrode/substrate, the dependence of the SERS response on the concentration of TBZ was assessed at − 0.8 V in PBS, pH 7. As shown in Fig. 2A, the intensity of characteristic TBZ SERS bands is well correlated with its concentration. Considering the band at 784 cm^{-1}, a linear regression (Y = 887.66 X + 462.48, r^2 = 0.9937) was obtained over a concentration range of 0.5–10 μM TBZ (Fig. 2B). The reproducibility of the recorded SERS signal was rather good (%RSD = 4.11, at 10 μM TBZ, n = 3), which, probably due to the less uniform adsorption of the pesticide molecule on the nanostructured surface, worsened towards the lower limit of the linear range (%RSD = 15.19, at 0.5 μM TBZ, n = 3). The LOD was estimated based on the noise recorded in the two tested matrices (PBS and juice) at 784 cm^{-1}. The LOD (3.3 * s_0/S) was calculated using the standard deviation of the recorded blank signal at 784 cm^{-1} (s_0, n = 5) and slope (S) of the calibration curve. The limits were found to be 0.27 μM (0.054 ppm) and 0.306 μM (0.061 ppm) for TBZ in PBS and in apple juice respectively, being lower than the MRL level.

To assess the suitability of the developed sensor for rapid analysis in real sample matrices, commercial apple juice was spiked with two different concentrations of TBZ and tested by EC-SERS at − 0.8 V. The matrix effect is a real problem in direct SERS analysis of foods (Huang, Wang, Lai, Fan, & Rasco, 2020; Zhang et al., 2021) since in the absence of any kind of sample pretreatment various matrix components may adsorb preferentially on the surface of the nanostructured SERS substrates and hinder the signal of the analyte. Moreover, interference from vibrational band overlaps is another important source or error. Hence, additional pretreatment steps are usually applied before the detection of pesticides from various food samples, making the method prone to systematic errors and more difficult to apply for on-site detection.

The suitability of the 784 cm^{-1} TBZ band for measurements in unprocessed apple juice samples was assessed by comparing the SERS spectra of TBZ-free and TBZ spiked apple juice samples with standard working solutions in PBS. As it can be observed, apple juice components add some extra vibrational bands to the spectra (Fig. 2C), but none are overlapping with the characteristic TBZ bands, creating the premise for the direct EC-assisted SERS analysis of unprocessed apple juice samples. Additionally, at the optimum potential (−0.8 V) the matrix did not hinder dramatically the interaction of TBZ with the gold substrate. Consequently, the recovery of TBZ in juice samples at the two tested concentrations was found to be over 82 % (Table 1). Even if due to the matrix effect TBZ levels are slightly underestimated in real juice samples

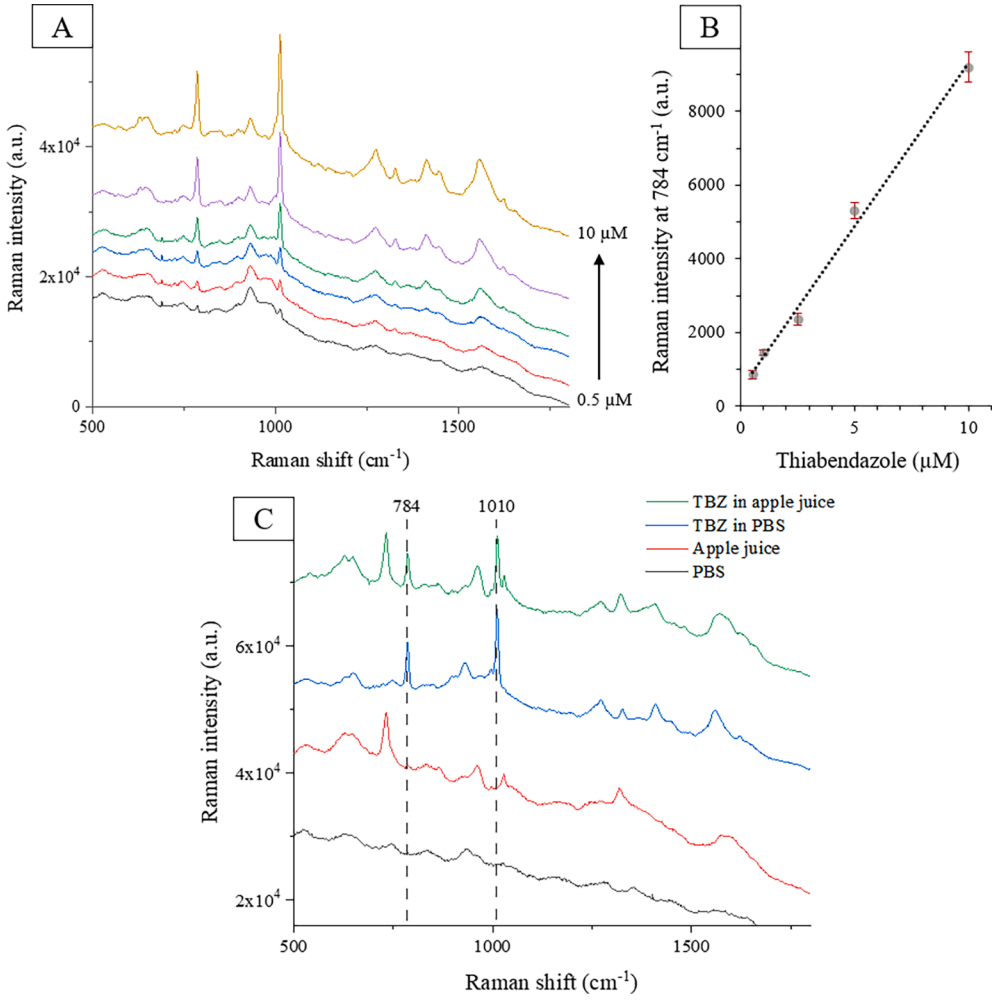

Fig. 2. Concentration dependence of the SERS signal of TBZ in PBS, pH 7, at −0.8 V (A); calibration curve for TBZ in PBS, pH 7 (B) and SERS spectra of TBZ in the unprocessed apple juice sample compared to its spectra in PBS (C).

Table 1
Recovery of TBZ from apple juice.

Sample	Spiked (M)	Quantified (M)	Recovery (%)	% RSD*
TBZ in PBSTBZ in PBS	7.5×10^{-7}	7.32×10^{-7}	97.61	4.45
	7.5×10^{-6}	7.62×10^{-6}	101.6	1.56
TBZ in apple juiceTBZ in apple juice	7.5×10^{-7}	6.51×10^{-7}	86.91	9.07
	7.5×10^{-6}	6.17×10^{-6}	82.26	4.65

*n = 3.

in comparison with the standard working solutions in PBS (97.6–101.6 %), these results may still be considered more than acceptable for a very fast (1 min total analysis time) and selective, direct spectroelectrochemical analysis of TBZ in apple juice. The previously reported SERS detection of TBZ from juice samples usually require more complex instrumentation, substrates, and sample processing, leading to longer analytical procedures for similar or sometimes worse analytical performances (Table 2). Therefore, the proposed EC-assisted SERS technique using mass-produced, easily accessible AuSPEs as electrode/substrate could be readily applied for the fast analysis of TBZ residues in unprocessed juice samples.

3.4. Microfluidic flow cell

Miniaturized analytical systems can bring a series of advantages (Langer et al., 2020), such as improved reproducibility due to the controlled reaction conditions, sometimes shortened detection times, automation of testing procedure and straightforward exchange of reagents (including reoccurring washing steps that may be required between sensor readings), potential for multiplexed tests, portability necessary for point-of-use systems, sustainability due to the reduced and smartly collected waste, and many other. In line with the current trend in food and environmental monitoring more efforts are made for integration of sensor devices with microfluidics to enable autonomous online sensing. An EC-SERS sensor could benefit from all of the above mentioned advantages. To the best of our knowledge, till date, only two such sensors were reported for uric acid (Huang & Hsiao, 2020) and metalloporphyrin hemin (Yuan et al., 2015) detection. Accurate sample delivery and integrated sample preparation approaches enabled by microfluidics may be exploited for in situ sample processing and/or preconcentration (Sun et al., 2020). Analyte molecules may be adsorbed from the passing flow onto the SERS electrode/substrate if they have intrinsic affinity towards gold and/or if the substrate is functionalized. Functionalization can be introduced by electrodeposition, with a corresponding layer of adsorbent, such as a thin layer of polymer or a thiolic or aminic self-assembled monolayer (SAM) (Pilot et al., 2019). There are contradicting reports concerning the TBZ affinity to metal nanostructures, some claiming that it has no affinity (Ding et al., 2019), whereas others indicate that TBZ induces the aggregation of metal nanoparticles (Oliveira et al., 2020).

To demonstrate that the developed EC-SERS sensor is functional when integrated in a microfluidic cell, a corresponding flow cell has been fabricated (see section 2.4) and tested under different experimental conditions for the analysis of TBZ. Flowing 10^{-5} M TBZ solution over the AuSPEs substrate at 15 μL/min resulted in a continuous enhancement of the specific TBZ Raman bands, without reaching a plateau upon 30 min of testing (Fig. 3). The time dependent increase in intensity of the TBZ's characteristic vibrational bands at 786 cm^{-1} and 1012 cm^{-1} (Fig. 4A) of approx. 20 and 40 times indicate an increasing number of pesticide molecules interacting with the gold surface. Another sensor was exposed for 30 min to the same concentration of TBZ without flow, observing nearly the halving of Raman band intensity (Fig. 4B) due to surface heating and TBZ desorption. This data demonstrates that under flow conditions TBZ molecules may indeed be preconcentrated through an adsorption mechanism on the gold surface without any prior surface functionalization steps. For this reason, the time of spectra recording should be carefully considered and controlled for quantitative analysis and the laser should only be on when recording relevant spectra since it can have a mitigating effect on TBZ signal. The signal recorded for the same concentration of TBZ was 2–3 times lower in flow cell assembly as opposed to the O-ring configuration most probably due to a different optical path of the laser beam that passed through the PPMA lid and

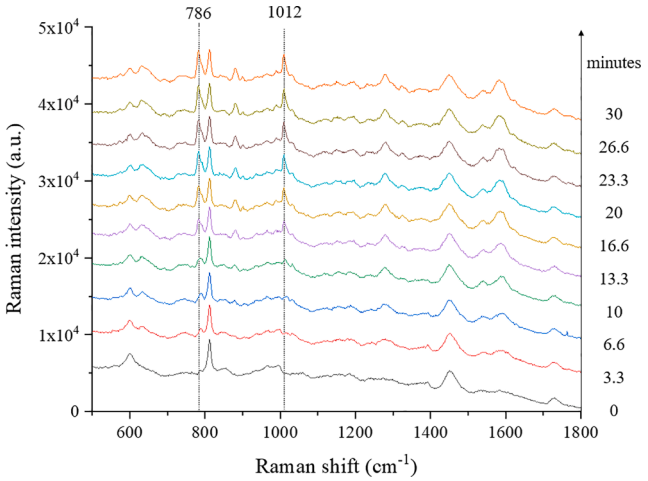

Fig. 3. Spectra representing the SERS signal of 10^{-5} M TBZ on AuSPEs integrated in a miniaturized chamber, collected over 30 min at 15 μL/min flow rate.

Table 2
Previously reported SERS sensors for TBZ in juice.

Substrate	Juice matrix	LOD (ppm)	Recovery (%)	Processed sample	Processing and analysis time (min)	Microscope	Wavelength (nm)	Laser power (mW)	Ref.
vertically aligned AuNR arrays	lemon carrot mango	0.149 0.216 0.179	96 – 98 97 – 99 96	yes	18	yes	785	20	(Alsammarraie et al., 2018)
Ag colloid	orange	4	87.2 – 108.8	yes	23	yes	785	25	(Feng et al., 2018)
Au@Ag NRs	apple peach	0.032 0.034	98.2 – 100.5 94.9 – 98.8	yes	greater than10	no	785	140	(Chen et al., 2022)
Au@Ag nanodot array	pear apple orange	0.051	76 – 105 88 – 126 82–131	yes	60	yes	633	4.25	(Wang, Sun, Pu, & Wei, 2020)
Activated AuSPEs	apple	0.061	82 – 86.91	no	1	no	785	68	This work

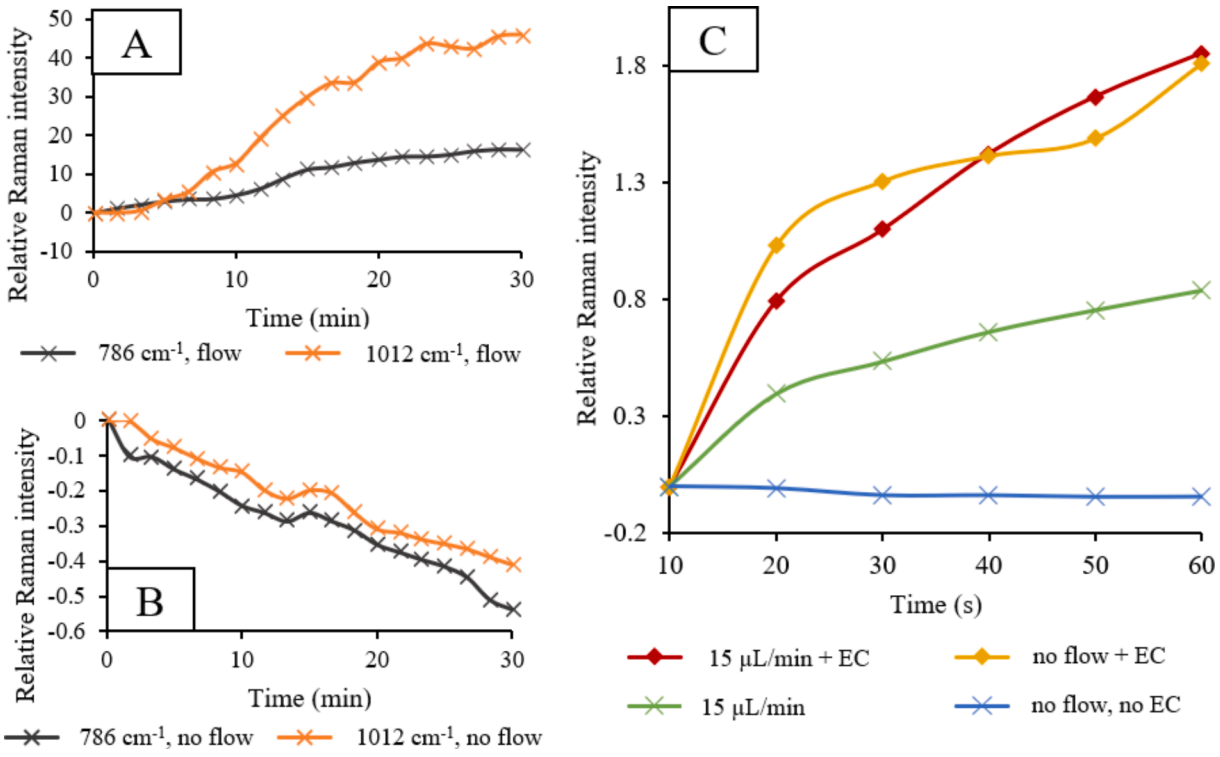

Fig. 4. Relative Raman intensity for two characteristic vibrational bands of TBZ recorded at 15 µL/min (A) and without flow (B) over 30 min; comparison of Raman intensity at 784 cm^{-1} for different EC-SERS microfluidic conditions (C).

affected the SERS readout. For the same reason and added limitations in synchronization between the syringe pump, EC and SERS readouts, the signal recorded for the same concentration of TBZ on different integrated electrodes varied. Therefore, the relative variation of the signal was presented to compare these data. The setup needs to be further optimized in future studies.

Additional studies were conducted to investigate the effect of EC potential (−0.8 V) on the sensors assembled in flow cells. In no-flow conditions, the enhancement at 784 cm^{-1} induced by the electrode polarization (Fig. 4C, yellow) can be clearly seen in contrast to the absence of electrode polarization (Fig. 4C, blue) when a continuous decrease of TBZ signal is recorded. At a flow rate of 15 µL/min (Fig. 4C, red) the signal increase is generated by the EC potential similarly to what has been shown for the no-flow conditions. The comparison between flow and no flow condition is done during the first minute when there is no significant adsorption of TBZ. Therefore, in a miniaturized cell, a flow rate can help preconcentrate TBZ molecules and an EC potential applied has a beneficial enhancing effect, leading to potential applications for the ultratrace analysis of TBZ, for example, in surface waters.

4. Conclusion

An EC-assisted SERS method was developed for simple, fast, and selective detection of residual TBZ directly from unprocessed apple juice samples. The commercially available AuSPEs proved to be convenient and cost-effective alternative EC-SERS substrates after a suitable EC activation procedure. The total analysis required only two minutes, including the substrate activation by EC roughening. An optimum potential applied to the electrode/substrate improved the recorded SERS signal, leading to similar or improved analytical performance over previously reported SERS sensors for TBZ analysis. The LOD of the proposed EC-assisted SERS method reaches down to 0.061 ppm TBZ in juice which is relevant for its trace detection in food samples, meeting the MRL levels. Acceptable recovery (>82 %) of TBZ was obtained in spiked apple juice samples. Furthermore, as a proof-of-concept the EC-SERS sensors were assembled into miniaturized flow cells and preliminary evaluation of their performance under flow conditions was also demonstrated. In the future, integration of EC-SERS sensors with microfluidics may enable a fully portable system for real-time monitoring of potential pesticide contamination in various environmental samples and for the decentralized food safety management.

Funding

The research leading to these results has received funding from the Norway Grants 2014–2021, under Project contract no. 32/2020.

CRediT authorship contribution statement

Rebeca Moldovan: Conceptualization, Data curation, Investigation, Methodology, Formal analysis, Writing – original draft, Writing – review & editing. **Karolina Milenko:** Data curation, Investigation, Methodology, Formal analysis, Writing – original draft, Writing – review & editing. **Elizaveta Vereshchagina:** Conceptualization, Data curation, Investigation, Methodology, Formal analysis, Resources, Writing – original draft, Writing – review & editing. **Bogdan-Cezar Iacob:** Data curation, Methodology, Formal analysis. **Kenneth Schneider:** Methodology, Formal analysis. **Cosmin Farcău:** Conceptualization, Data curation, Methodology, Formal analysis, Resources, Writing – original draft, Writing – review & editing. **Ede Bodoki:** Conceptualization, Methodology, Resources, Writing – review & editing.

Declaration of Competing Interest

The authors declare that they have no known competing financial interests or personal relationships that could have appeared to influence the work reported in this paper.

Data availability

Data will be made available on request.

Acknowledgements

The authors thank L. Barbu-Tudoran for electron microscopy analyses. J. Batalden (SINTEF AS) is acknowledged for his help with milling of prototypes for assembly of microfluidic devices.

Appendix A. Supplementary data

Supplementary data to this article can be found online at https://doi.org/10.1016/j.foodchem.2022.134713.

References

Abad, A., Manclús, J. J., Moreno, M. J., & Montoya, A. (2001). Determination of thiabendazole in fruit juices by a new monoclonal enzyme immunoassay. *Journal of AOAC International, 84*(1), 156–161.

Albero, B., Sánchez-Brunete, C., & Tadeo, J. L. (2004). Determination of thiabendazole in orange juice and rind by liquid chromatography with fluorescence detection and confirmation by gas chromatography/mass spectrometry after extraction by matrix solid-phase dispersion. *Journal of AOAC International, 87*(3), 664–670.

Alsammarraie, F. K., Lin, M., Mustapha, A., Lin, H., Chen, X., Chen, Y., … Huang, M. (2018). Rapid determination of thiabendazole in juice by SERS coupled with novel gold nanosubstrates. *Food Chemistry, 259*, 219–225. https://doi.org/10.1016/j.foodchem.2018.03.105

Aroca, R. (2007). Theory of Molecular Vibrations. The Origin of Infrared and Raman Spectra. *Surface-Enhanced Vibrational Spectroscopy*, 1–33. https://doi.org/10.1002/9780470035641.CH1

Bindesri, S. D., Alhatab, D. S., & Brosseau, C. L. (2018). Development of an electrochemical surface-enhanced Raman spectroscopy (EC-SERS) fabric-based plasmonic sensor for point-of-care diagnostics. *Analyst, 143*(17), 4128–4135. https://doi.org/10.1039/C8AN01117F

Bindesri, S. D., Jebailey, R., Albarghouthi, N., Pye, C. C., & Brosseau, C. L. (2020). Spectroelectrochemical and computational studies of tetrahydrocannabinol (THC) and carboxy-tetrahydrocannabinol (THC-COOH). *Analyst, 145*(5), 1849–1857. https://doi.org/10.1039/C9AN02173F

Chen, Z., Sun, Y., Shi, J., Zhang, W., Zhang, X., Huang, X., … Wei, R. (2022). Facile synthesis of Au@Ag core–shell nanorod with bimetallic synergistic effect for SERS detection of thiabendazole in fruit juice. *Food Chemistry, 370*, Article 131276. https://doi.org/10.1016/j.foodchem.2021.131276

Ding, Q., Kang, Z., He, X., Wang, M., Lin, M., Lin, H., & Yang, D.-P. (2019). Eggshell membrane-templated gold nanoparticles as a flexible SERS substrate for detection of thiabendazole. *Microchimica Acta, 186*(7), 453. https://doi.org/10.1007/s00604-019-3543-1

EPA Office of Pesticide Programs, U. (n.d.). *US EPA - Pesticides - Reregistration Eligibility Decision (RED) for Thiabendazole*.

EU Pesticides Database. (n.d.). Retrieved August 19, 2022, from https://food.ec.europa.eu/plants/pesticides/eu-pesticides-database_en.

Feng, J., Hu, Y., Grant, E., & Lu, X. (2018). Determination of thiabendazole in orange juice using an MISPE-SERS chemosensor. *Food Chemistry, 239*, 816–822. https://doi.org/10.1016/j.foodchem.2017.07.014

Hassanain, W. A., Izake, E. L., & Ayoko, G. A. (2018). Spectroelectrochemical Nanosensor for the Determination of Cystatin C in Human Blood. *Analytical Chemistry, 90*(18), 10843–10850. https://doi.org/10.1021/acs.analchem.8b02121

Hernandez, S., Perales-Rondon, J. V., Heras, A., & Colina, A. (2019). Determination of uric acid in synthetic urine by using electrochemical surface oxidation enhanced Raman scattering. *Analytica Chimica Acta, 1085*, 61–67. https://doi.org/10.1016/j.aca.2019.07.057

Huang, C.-Y., & Hsiao, H.-C. (2020). Integrated EC-SERS Chip with Uniform Nanostructured EC-SERS Active Working Electrode for Rapid Detection of Uric Acid. *Sensors, 20*(24), 7066. https://doi.org/10.3390/s20247066

Huang, Y., Wang, X., Lai, K., Fan, Y., & Rasco, B. A. (2020). Trace analysis of organic compounds in foods with surface-enhanced Raman spectroscopy: Methodology, progress, and challenges. *Comprehensive Reviews in Food Science and Food Safety, 19*(2), 622–642. https://doi.org/10.1111/1541-4337.12531

Ibáñez, D., González-García, M. B., Hernández-Santos, D., & Fanjul-Bolado, P. (2021). Detection of dithiocarbamate, chloronicotinyl and organophosphate pesticides by electrochemical activation of SERS features of screen-printed electrodes. *Spectrochimica Acta Part A: Molecular and Biomolecular Spectroscopy, 248*, Article 119174. https://doi.org/10.1016/j.saa.2020.119174

Kim, M. S., Kim, M. K., Lee, C. J., Jung, Y. M., & Lee, M. S. (2009). Surface-enhanced Raman spectroscopy of benzimidazolic fungicides: Benzimidazole and thiabendazole. *Bulletin of the Korean Chemical Society, 30*(12), 2930–2934. https://doi.org/10.5012/bkcs.2009.30.12.2930

Langer, J., Jimenez de Aberasturi, D., Aizpurua, J., Alvarez-Puebla, R. A., Auguié, B., Baumberg, J. J., … Liz-Marzán, L. M. (2020). Present and Future of Surface-Enhanced Raman Scattering. *ACS Nano, 14*(1), 28–117. https://doi.org/10.1021/acsnano.9b04224

Liu, Y., Zhang, Y., Tardivel, M., Lequeux, M., Chen, X., Liu, W., … Fu, W. (2020). Evaluation of the Reliability of Six Commercial SERS Substrates. *Plasmonics, 15*(3), 743–752. https://doi.org/10.1007/s11468-019-01084-8

Lynk, T. P., Sit, C. S., & Brosseau, C. L. (2018). Electrochemical Surface-Enhanced Raman Spectroscopy as a Platform for Bacterial Detection and Identification. *Analytical Chemistry, 90*(21), 12639–12646. https://doi.org/10.1021/acs.analchem.8b02806

Mohammadniaei, M., Yoon, J., Lee, T., & Choi, J. W. (2018). Spectroelectrochemical detection of microRNA-155 based on functional RNA immobilization onto ITO/GNP nanopattern. *Journal of Biotechnology, 274*, 40–46. https://doi.org/10.1016/j.jbiotec.2018.03.014

Müller, C., David, L., Chiş, V., & Pînzaru, S. C. (2014). Detection of thiabendazole applied on citrus fruits and bananas using surface enhanced Raman scattering. *Food Chemistry, 145*, 814–820. https://doi.org/10.1016/j.foodchem.2013.08.136

Oliveira, M. J. S., Rubira, R. J. G., Furini, L. N., Batagin-Neto, A., & Constantino, C. J. L. (2020). Detection of thiabendazole fungicide/parasiticide by SERS: Quantitative analysis and adsorption mechanism. *Applied Surface Science, 517*, Article 145786. https://doi.org/10.1016/j.apsusc.2020.145786

Pesticide Residue Monitoring Report and Data for FY 2019 | FDA. (n.d.). Retrieved August 19, 2022, from https://www.fda.gov/food/pesticides/pesticide-residue-monitoring-report-and-data-fy-2019.

Pilot, R., Signorini, R., Durante, C., Orian, L., Bhamidipati, M., & Fabris, L. (2019). A Review on Surface-Enhanced Raman Scattering. *Biosensors, 9*(2). https://doi.org/10.3390/bios9020057

Revision of the review of the existing maximum residue levels for thiabendazole. (2016). *EFSA Journal, 14*(6). doi:10.2903/J.EFSA.2016.4516.

Robinson, A. M., Harroun, S. G., Bergman, J., & Brosseau, C. L. (2012). Portable Electrochemical Surface-Enhanced Raman Spectroscopy System for Routine Spectroelectrochemical Analysis. *Analytical Chemistry, 84*(3), 1760–1764. https://doi.org/10.1021/ac2030078

Ru, E. L., & Etchegoin, P. (2008). *Principles of Surface-Enhanced Raman Spectroscopy and Related Plasmonic Effects* (1st ed.). Elsevier B.V.

Salinas-Torres, D., Huerta, F., Montilla, F., & Morallón, E. (2011). Study on electroactive and electrocatalytic surfaces of single walled carbon nanotube-modified electrodes. *Electrochimica Acta, 56*(5), 2464–2470. https://doi.org/10.1016/J.ELECTACTA.2010.11.023

Sannino, A. (2008). Chapter 9 Pesticide Residues. *Comprehensive Analytical Chemistry, 51*, 257–305. https://doi.org/10.1016/S0166-526X(08)00009-3

Sarfo, D. K., Izake, E. L., O'Mullane, A. P., Wang, T., Wang, H., Tesfamichael, T., & Ayoko, G. A. (2019). Fabrication of dual function disposable substrates for spectroelectrochemical nanosensing. *Sensors and Actuators B: Chemical, 287*, 9–17. https://doi.org/10.1016/j.snb.2019.02.012

Sun, J., Gong, L., Wang, W., Gong, Z., Wang, D., & Fan, M. (2020). Surface-enhanced Raman spectroscopy for on-site analysis: A review of recent developments. *Luminescence, 35*(6), 808–820. https://doi.org/10.1002/bio.3796

Velička, M., Zacharovas, E., Adomavičiūtė, S., & Šablinskas, V. (2021). Detection of caffeine intake by means of EC-SERS spectroscopy of human saliva. *Spectrochimica Acta Part A: Molecular and Biomolecular Spectroscopy, 246*, Article 118956. https://doi.org/10.1016/j.saa.2020.118956

Wang, K., Sun, D.-W., Pu, H., & Wei, Q. (2020). Two-dimensional Au@Ag nanodot array for sensing dual-fungicides in fruit juices with surface-enhanced Raman spectroscopy technique. *Food Chemistry, 310*, Article 125923. https://doi.org/10.1016/j.foodchem.2019.125923

Wu, D.-Y., Li, J.-F., Ren, B., & Tian, Z.-Q. (2008). Electrochemical surface-enhanced Raman spectroscopy of nanostructures. *Chemical Society Reviews, 37*(5), 1025–1041. https://doi.org/10.1039/b707872m

Yuan, T., Le Thi Ngoc, L., van Nieuwkasteele, J., Odijk, M., van den Berg, A., Permentier, H., … Carlen, E. T. (2015). In Situ Surface-Enhanced Raman Spectroelectrochemical Analysis System with a Hemin Modified Nanostructured Gold Surface. *Analytical Chemistry, 87*(5), 2588–2592. https://doi.org/10.1021/ac504136j

Zhang, D., Liang, P., Chen, W., Tang, Z., Li, C., Xiao, K., … Yu, Z. (2021). Rapid field trace detection of pesticide residue in food based on surface-enhanced Raman spectroscopy. *Microchimica Acta, 188*(11), 370. https://doi.org/10.1007/s00604-021-05025-3

Zhao, L., Blackburn, J., & Brosseau, C. L. (2015). Quantitative Detection of Uric Acid by Electrochemical-Surface Enhanced Raman Spectroscopy Using a Multilayered Au/Ag Substrate. *Analytical Chemistry, 87*(1), 441–447. https://doi.org/10.1021/ac503967s